SURFACE DESIGN FOR DROPWISE CONDENSATION: A THEORETICAL AND EXPERIMENTAL STUDY

Ahlers M.[1], Koch M.[2], Lägel B.[3], Klingel S.[3], Schlehuber D.[4], Gehrke I.[4], Eloo C.[4], Bart H.-J.[1*]
*Author for correspondence
[1]Chair of Separation Science and Technology, TU Kaiserslautern, Kaiserslautern
[2]INM – Leibniz Institute for New Materials, Saarbrücken
[3]Nano Structuring Center, TU Kaiserslautern, Kaiserslautern
[4]Fraunhofer Institute for Environmental, Safety, and Energy Technology UMSICHT, Oberhausen
Germany
E-mail: bart@mv.uni-kl.de

ABSTRACT

The manipulation of the water wetting properties of heat exchangers into dropwise condensation by the use of microstructured surfaces promises an enhanced heat transfer. In order to design a hydrophobic surface geometry, different theoretical models have been introduced in the past. While these models describe the surface-drop-interaction of sessile drops reasonably well, nucleation and droplet growth in dropwise condensation are not considered. Modifications of roughness based models have been introduced as quantitative surface structure design guidelines. The theory of local energy barriers has been contrived and dependencies on the bond number and solid-liquid fraction have been found.

This study aims at validating these theoretical models and their applicability for the design of hydrophobic surfaces used for dropwise condensation. To gain deeper understanding of the underlying mechanism of dropwise condensation silicon-nanopillars of five microns height, different diameter (several hundred nanometers) and pillar distance (below two microns) were fabricated in a cryogenic deep reactive-ion etching process. The influence of material properties on the wetting behavior was simulated by using coatings with different intrinsic contact angles (silicon dioxide, Parylene C, octafluorocyclobutane) on the microstructures. The intrinsic advancing contact angle and the surface geometry showed a strong influence on the droplet formation. The investigated theoretical models were not fully coherent with gained experimental data. The experimental results and theoretical simulations show that a simple and conclusive model is yet to be found that describes the droplet-surface interaction during dropwise condensation.

INTRODUCTION

Condensation of vapor is a crucial part of many industrial processes such as desalination, power generation and refrigeration. Depending on the wettability of the surface the condensate accumulates as a film or a drop. Whereas film condensation is the common mode of condensation found in applications, Schmidt et al. recognized dropwise condensation to have a higher heat transfer efficiency in 1930 [1]. Imperative of dropwise condensation is a (super-) hydrophobic surface, indicated by a high contact angle and low contact angle hysteresis to sweep condensing drops easily.

The drop-surface interaction on smooth surfaces was first described by Young, who related the surface tensions between the three phases solid, liquid and gas [2]. Since most smooth materials are hydrophilic and fail to show contact angles above 90°, surface structures can enhance their hydrophobic behavior, as seen on many surfaces in nature [3–7]. However, not every structure exhibits desired effects. The petal and lotus effect describe generally known phenomena. The petal effect implies sessile drops with high contact angles penetrating the surface structure. This results in adhesive drops sticking to the surface [8,9]. Wenzel related Young's contact angle with a surface roughness factor to describe the apparent contact angle for adhesive, wetting drops on single-tier textured surfaces [10]. The lotus effect represents sessile drops, which sit suspended on the tips of the surface structure with a high contact angle and mobility [11,12]. Cassie & Baxter found an expression to describe the apparent contact angle for such non-wetting drops relating Young's contact angle with a solid-liquid-fraction [13].

Whereas the roughness based correlations of Wenzel and Cassie & Baxter are generally accepted to describe drop-surface-interactions, new studies question their validity for inhomogeneous surface structures. A dependency on the local three-phase contact line and the contact line density is proposed instead [14–17]. Furthermore, roughness based theories are limited to describing the drop-surface-interaction of sessile drops. Nonetheless, they serve as a basic principle to simulate droplet formation on structured surfaces during condensation. Nucleation sites, droplet growth and shedding, pinning and process parameters are not accounted for, which lead to incoherent experimental results with theory [18–21]. In the past years, researchers have tried to find correlations to include these effects in theoretical models and facilitate the surface structure design for stable dropwise condensation [22–24].

In this work, we study the influence of structure scaling and material properties during condensation to compare it with existing theoretical models for surface design. The surfaces tested include both smooth and textured silicon wafers. Three materials (either hydrophilic or hydrophobic) with different intrinsic advancing contact angles are investigated to visualize their influence on the wetting behavior during condensation. Experimental results are compared to existing models of Enright et al. [22] and Lo et al. [24].

NOMENCLATURE

Bo^*	[−]	modified Bond number
d	[m]	diameter
D	[m]	droplet departure diameter
E^*	[−]	dimensionless energy
f	[−]	solid-liquid fraction
g	[m/s²]	gravity
h	[m]	height
l	[m]	pillar distance (center to center)
r	[−]	roughness
x	[m]	pillar interspace (wall to wall)

Special characters

Δ	[−]	difference
θ	[°]	contact angle
ρ	[kg/m³]	density
σ	[N/m]	surface tension
ϕ	[°]	inclination angle
X	[−]	actual solid-liquid fraction

Subscripts

a	advancing
app	apparent
B	base
C	C_4F_8
$calc$	calculated
D	drop
i	meaning a,r or s
P	Parylene C
r	receding
s	static
S	SiO_2
0	intrinsic

EXPERIMENTAL METHODS

Fabrication of Si-nanopillars

For the manufacturing of the samples a 100 nm thick oxide layer was grown on a 4 inch Si-wafer (CZ, 100, p-type) by thermal oxidation to serve as an etch mask for the Si pillars. After dicing the wafer 8 x 8 mm² chips were spin coated with ma-N2403 negative tone resist from Microresist Technology. A Raith e_LiNE electron beam lithography tool was then used to expose the resist with the various 200 x 200 µm² arrays of circles. Subsequent to the resist development in MIF726 (Micro-chemicals, Germany) the patterns were transferred into the oxide layer by Ar^+-ion beam etching (IBE) in a Roth & Rau Ionsys 500 at an incident angle of 70°. Before etching the pillars into the Si substrate the resist mask was removed with Technistrip P1316 (Microchemicals, Germany) resist stripper.

Cryogenic deep reactive-ion etching (DRIE) was performed in an Oxford Plasma Pro 100 Cobra ICP Etch with sulfur hexafluoride (SF_6). The Si substrates were then plasma cleaned with O_2 for 10 min at 100 W in a Diener Electronic PICO-UHP. Table 1 lists the details of the fabricated surfaces. Fig. 1 depicts the nanopillar arrays of the four investigated surface structures.

Table 1 Average Si-nanopillar dimensions (h ≈ 5.1 µm).

Structure field	d [µm]	l [µm]	x [µm]
F1	0.55	2.0	1.45
F2	0.55	1.0	0.45
F3	0.35	1.3	0.95
F4	0.35	0.9	0.55

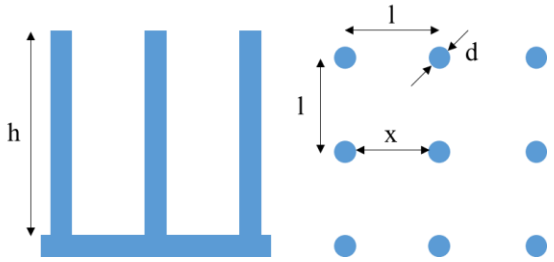

Figure 2 Schematic pillar array.

Coating of Si-substrate

Three surface materials were tested: silicon dioxide (SiO_2) as natural oxide layer on silicon, Parylene C (SCS, USA) and octafluorocyclobutane (C_4F_8 99%, Air Liquide, Germany). A thin layer of Parylene C was deposited on the Si sample via physical vapor deposition in a Parylene PVD-evaporator (SCS PDS 2010, Cookson Electronics, UK). A Roth & Rau MicroSys 350 reactive ion etcher (ECR-RIE) was used for the C_4F_8 functionalization. Layer thicknesses on smooth samples were determined to approximately 50 nm for both coatings. From visual validation of environmental scanning electron microscopy (ESEM) images, layer thickness is assumed to be smaller on textured surface.

Characterization of wetting properties

Condensation experiments were performed in a FEI Quanta 400 FEG ESEM with built-in cooling stage. Samples were attached with double sided carbon tape. A GSED detector was used for secondary electron detection mode. The substrate was cooled to 276 K at a pressure below the corresponding equilibrium water vapor pressure of 760 Pa for a minimum of 0.5 h. Increasing the water vapor pressure to 820-1100 Pa resulted in condensation of water onto the sample. Images were obtained at an inclination angle of 60 ° and acceleration voltage of 20 kV.

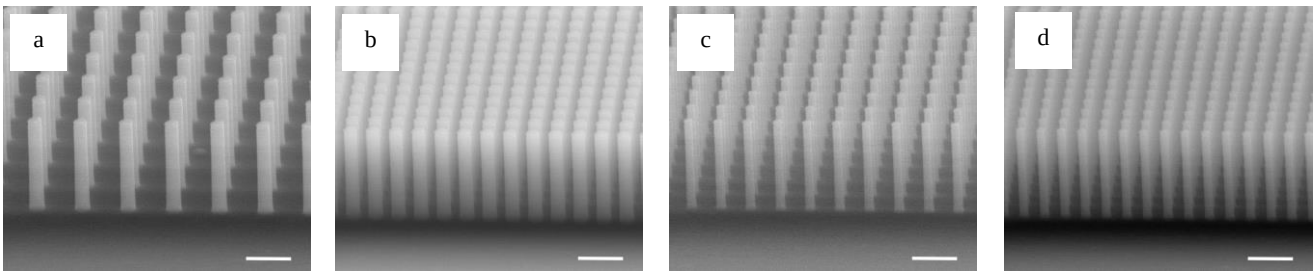

Figure 1 Nanopillars on structure fields F1 (a), F2 (b), F3 (c) and F4 (d). Scale bars = 2 µm .

Advancing, receding and static contact angles of sessile drops on smooth samples were measured with a goniometer (DataPhysics OCA 15 EC). Measured values for SiO_2, ParyleneC and C_4F_8 are $\theta_{a,0,S} = 64° \pm 0.5°$ / $\theta_{r,0,S} = 31° \pm 2.8°$ / $\theta_{s,0,S} = 61° \pm 0.2°$, $\theta_{a,0,P} = 87° \pm 3.1°$/ $\theta_{r,0,P} = 63° \pm 4.4°$ / $\theta_{s,0,P} = 76° \pm 3.8°$, $\theta_{a,0,C} = 120° \pm 0.5°$/$\theta_{r,0,C} = 96° \pm 0.3°$ / $\theta_{s,0,C} = 113° \pm 0.3°$, respectively. Advancing contact angles of condensed droplets on smooth and textured surfaces were estimated from ESEM images. It was assumed that gravitational forces can be neglected and droplets form a sphere. The contact angle was calculated from the droplet and the base diameter d_D and d_B of the droplet using

- for angles < 90° :

$$\theta_{a,app} = \sin^{-1}\left(\frac{d_B}{d_D}\right) \quad (1)$$

- for angles > 90° :

$$\theta_{a,app} = 180° - \sin^{-1}\left(\frac{d_B}{d_D}\right). \quad (2)$$

To identify the base diameter freshly nucleated, isolated, growing droplets with advancing contact angles > 90° were gradually evaporated and images superimposed (Fig. 3). For contact angles < 90° change in curvature was identified as diameter. A minimum of five droplets per surface structure and per material were utilized for visual contact angle estimation. The droplet diameter varied between 13-67 µm for smooth surfaces and 6-20 µm for textured surfaces. The advancing contact angle of droplets on smooth surfaces corresponded reasonably well to goniometric measurements on smooth surfaces. Contact angle deviations were generally accredited to accuracy differences between goniometric measurement and visual estimation. Different thicknesses of oxid layer due to exposure time to air on the Si-samples may have caused contact angle deviations of up to 10°. Apparent static and receding contact angles for droplets could not be estimated from ESEM images: the process was dynamic and visualized droplets generally showed receding contact angles of $\theta_{r,app} \approx 0°$ due to their size.

The actual solid liquid fraction X (eq. (7)) was determined from an image sequence of isolated nucleating, growing and evaporating droplets.

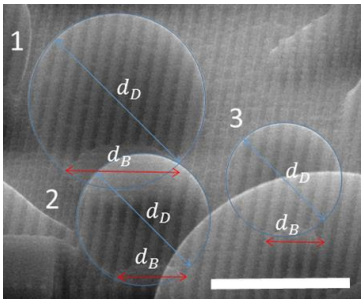

Figure 3 Superimposed images of growing and evaporating droplets for calculation of advancing contact angles with eq. (2). Scale bar = 20 µm.

THEORY FOR SURFACE DESIGN MODELS

Three types of droplets are commonly distinguished in dropwise condensation: wetting droplets (also known as Wenzel-droplets), suspended droplets (also known as Cassie-droplets) and hybrids of wetting and suspended droplets known as partially wetting droplets [23,25]. Miljkovic et al. found partially wetting droplets to be the most desirable type. They show weak pinning and a high heat transfer rate due to local wetting [25].

Apart from creating a water-repellent surface, surface structure can also manipulate the type of condensing droplets [22]. The complexity of dropwise condensation and its many influencing parameters complicates the development of a guideline for qualitative surface structure design. Quantitative surface design models were proposed by Enright et al. [22] and Lo et al. [24].

Enright et al. investigated wetting and partially wetting droplets on differently scaled nanopillar surfaces. Explanation of differing wetting behavior was found in terms of a non-equilibrium energy criterion. By comparing the dimensionless energy E^* for advancing wetting and suspended droplet states, the expected droplet morphology can be calculated with

$$E^* = \frac{-1}{r\cos\theta_{a,0}}, \quad (3)$$

where the roughness of a single-tier surface structure is the ratio of the total to projected surface area, determined by

$$r = \frac{l^2 + \pi dh}{l^2}. \quad (4)$$

With the dimensionless energy $E^* > 1$ wetting droplets are favored, with $E^* < 1$ partially wetting droplet morphologies should condense.

Lo et al. suggest a modified Bond number $Bo^* < 0.1$ and a small solid-liquid fraction < 0.3 as guideline for surface structure design. The modified Bond number is defined as

$$Bo^* = \frac{\rho g D^2}{\sigma f}, \quad (5)$$

where ρ is the density of the droplet, g the gravity, D the departure diameter, σ the surface tension and f the solid-liquid-fraction for a suspended drop. The solid-liquid fraction is defined as the ratio of the solid-liquid contact area to the projected solid surface area

$$f = \frac{\pi d^2}{4l^2}. \quad (6)$$

Gravitational shedding of droplets cannot be observed in the ESEM images due to visual limitation. Instead, the droplet departure diameter is calculated as suggested by Lo et al.:

$$D = 2\sqrt{\frac{3X\sigma\left(cos\theta_{app,r} - cos\theta_{app,a}\right)}{\rho g\left(2 - 3cos\theta_{app,s} + \cos^3\theta_{app,s}\right)cos\phi}}, \quad (7)$$

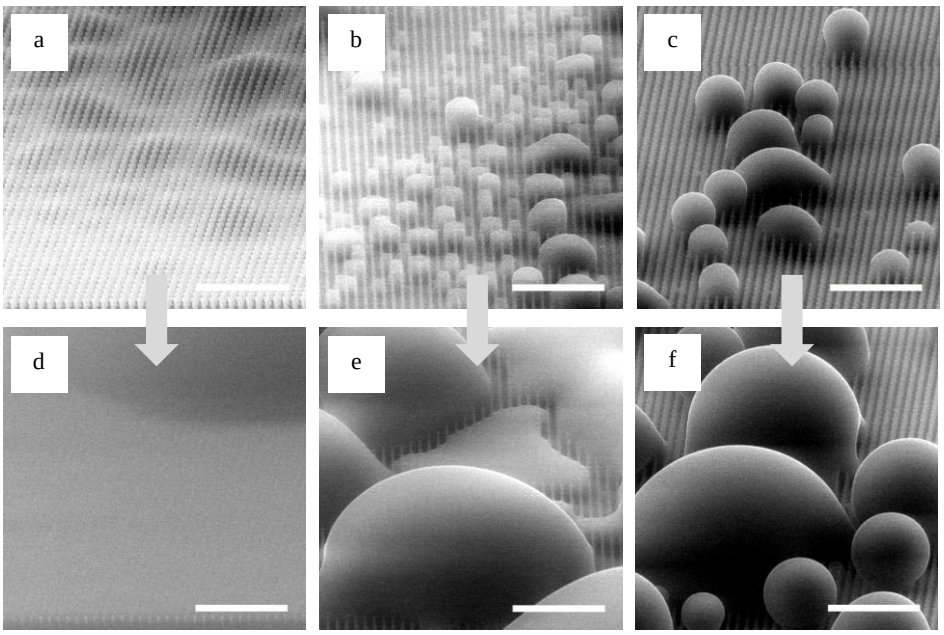

Figure 4 Surface material properties play an important role in wetting. Fig. a-c show initial droplet nucleation on structure field F1 for SiO_2, Parylene C and C_4F_8, respectively. Not only nucleation site and rate differ for the materials, but also droplet growth leading to flooded (d), partially flooded (e) and non-wetting (f) surfaces. Scale bars = 20 μm.

where X is the actual solid-liquid fraction, defined as the ratio of the actual solid-liquid contact area to the total solid surface area underneath the droplet for partially wetting droplets and ϕ is the inclination angle of the surface.

The apparent contact angles of suspended drops were calculated from the instrinsic contact angles with the correlation expressed by Cassie & Baxter [13]:

$$cos\theta_{i,app} = f\left(cos\theta_{i,0} + 1\right) - 1\,. \qquad (8)$$

RESULTS AND DISCUSSION

Influence of material on wetting characteristics

Chosen materials show different wettability. Whereas SiO_2 is hydrophilic, Parylene C has a decreased wettability and C_4F_8 is hydrophobic. Surface structures can enhance the water repellency even for hydrophilic materials with low intrinsic contact angles. Fig. 4 shows the wetting behavior on structure field F1 for SiO_2, Parylene C and C_4F_8 after droplet nucleation (Fig. 4a-c) and after coalescence processes (Fig. 4d-f).

On SiO_2 water condenses between the nanopillars forming droplets with low contact angles similar to contact angles on the smooth surface (Fig. 4a). Pinning on nanopillars within the structure does not occur. Only at the border of the structure field water rather pins to the pillars than wets surrounding smooth areas, presumably due to capillary effects. Once the structure is completely flooded with water a drop grows atop (Fig. 4d).

Parylene C has almost hydrophobic properties. It allows nucleated droplets to form water bridges and gradually fill 2x2 unit cells before growing above the surface structure (Fig. 4b). However, the many nucleation sites result in coalescence of the droplets before they can fully develop. It seems energetically more favorable for droplets to coalesce between nanopillars than on top of the surface structure. Hence, collapse of the coalescing droplets and local flooding can be observed (Fig. 4e). Flooded areas eventually form new droplets.

On C_4F_8 nucleation sites are wider spread compared to SiO_2 and Parylene C (Fig. 4c). This allows isolated droplets to grow to a diameter of 6-25 μm before coalescing with neighboring drops. Similar to wetting on Parylene C coated nanopillars, droplets initially wet liquid stems of approximately 2x2 unit cells before growing atop the surface structure. The partially wetting drops keep their base area after coalescence, which leads to deformed droplets. It is not evident from the image material if the area underneath the coalesced droplet stays dry or if the water penetrates the surface structure underneath the newly formed droplet. Even after coalescence, droplet formation seems stable.

Material properties appear to influence the nucleation sites and nucleation density as well as pinning behavior.

Influence of structure scaling

The fabricated surface structures vary in pillar diameter and pillar distance. ESEM images reveal a change in wettability even

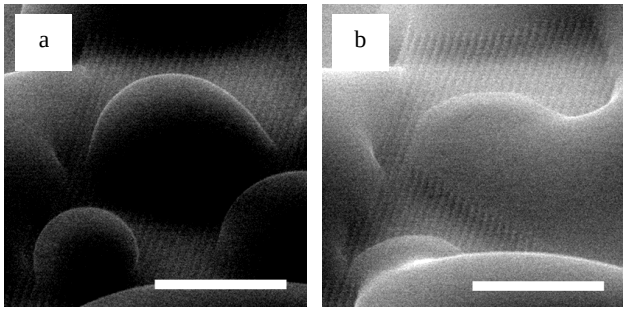

Figure 5 Condensing droplets on SiO_2 grow above the pillar array on structure field F3 (a). However, droplets are not stable and collapse between nanopillars after coalescence (b). Scale bars 20 μm.

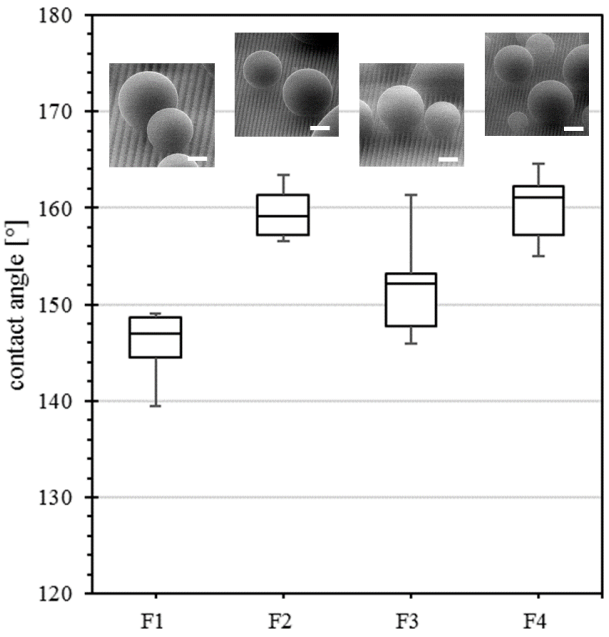

Figure 6 Apparent advancing contact angles $\theta_{a,app}$ on C_4F_8 coated structure fields F1, F2, F3 and F4. Scale bars 5 µm.

for the hydrophilic surface material SiO_2. Depending on the structure scaling, droplets can grow above the nanopillars as depicted in Fig. 5a for SiO_2. However, the droplets are not stable and collapse after coalescence (Fig. 5b). The Parylene C coated surface structure F1 shows similar behavior (Fig. 4b,e). The finer the structures (F2-F4) the more stable the droplets seem to become on Parylene C coated samples. In general, investigated geometries seem too coarse for stable dropwise condensation on both SiO_2 and Parylene C.

The contrary can be observed on C_4F_8 coated structured surfaces. All geometries show stable droplet formation. Droplets only differ in wetting behavior and contact angle (Fig. 6). On surface structures F1 and F3 droplets grow as partially wetting droplets. On surface structures F2 and F4 droplets also grow suspended on nanopillars. Advancing contact angles vary with wall-to-wall distance x of pillars (Tab. 1). Droplets on denser pillar arrays (F2 and F4) show higher advancing contact angles and the coalescence length seems to be reduced.

Validation of surface design models

Investigated surface samples are modeled as single-tier structures. This section solely considers C_4F_8 coated nanopillars.

Tab. 2 lists the results for the dimensionless energy E^* calculated with eq. (3). For all surface structures calculated values are < 1. Hence, partially wetting droplets are predicted. This is consistent with ESEM experiments. Surfaces with the lowest dimensionless energy E^* achieve the highest advancing contact angles in the condensation experiments. However, the model is only applicable for intrinsic contact angles > 90°.

The model of Lo et al. reveals incoherent results with experimental data (Tab. 3). Although the magnitude of calculated contact angles is in agreement with the experimentally observed wetting behavior, only the solid-liquid-fraction falls into the proposed range of $f < 0.3$.

The modeling of the surface structure as well as the estimation of the actual solid-liquid-fraction X are possible sources of error. While the surface is assumed as single-tier surface for the calculations, SEM images reveal a nano-roughness on the pillars with irregularities of up to 20 nm in height. According to the model of Lo at al., the actual solid-liquid-fraction X is independent of droplet growth. However, change of the base diameter and wetting behavior was observed in the ESEM experiments.

Investigated models are to use with caution. Simplifications and unconsidered droplet growth mechanisms can lead to faulty estimations.

Table 2 Calculations of r and E^* with eq. (3) and (4). Average dimensions for C_4F_8 coated nanopillars.

Structure field	d [µm]	l [µm]	h [µm]	r [µm]	E^* [-]
F1	0.60	2.0	5.06	3.4	0.6
F2	0.59	1.0	5.05	10.4	0.2
F3	0.37	1.3	5.10	4.5	0.4
F4	0.35	0.9	5.00	7.9	0.3

CONCLUSION

ESEM images of dropwise condensation reveal a material and structure scaling dependency for droplet formation. The nucleation density decreases with increasing hydrophobicity of the material. The wetting behavior of the material in combination with structure scaling changes the droplet type from wetting to suspended droplets. Concomitant, pinning seems to intensify and contact angles increase.

Proposed surface structure design models of Enright et al. and Lo et al. give a vague indication of whether the designed surface is suitable for dropwise condensation. The complex underlying mechanisms during dropwise condensation are not sufficiently incorporated into the models to give distinctive predictions.

Table 3 Calculations of f and Bo^* with eq. (5) - (8). Surface assumed as vertical ($\phi = 0°$).

Structure field	d [µm]	l [µm]	h [µm]	$\theta_{a,calc,C}$ [°]	$\theta_{r,calc,C}$ [°]	$\theta_{s,calc,C}$ [°]	X [-]	D [µm]	f [-]	Bo^* [-]
F1	0.60	2.0	5.06	165	159	163	0.81	731	0.07	0.98
F2	0.59	1.0	5.05	150	139	146	0.73	1372	0.27	0.90
F3	0.37	1.3	5.10	166	161	164	1.00	766	0.06	1.21
F4	0.35	0.9	5.00	160	153	158	0.85	980	0.12	1.04

ACKNOWLEDGEMENTS

The Authors would like to thank the Bundesministerium für Wirtschaft (German Federal Ministry for Economic Affairs) via the Arbeitsgemeinschaft Industrieller Forschungsgesellschaften (AiF) for financial support of the AiF project No. 18795 N.

REFERENCES

[1] E. Schmidt, W. Schurig, and W. Sellschopp, "Versuche über die Kondensation von Wasserdampf in Film- und Tropfenform," *VDI-Zeitschrift*, vol. 2, no. 1, pp. 53–63, 1930.

[2] T. Young, "An essay on the cohesion of fluids," *Phil. Trans. Royal Soc. London*, vol. 95, pp. 65–87, 1805.

[3] E. Bormashenko, Y. Bormashenko, T. Stein et al., "Why do pigeon feathers repel water? Hydrophobicity of pennae, Cassie-Baxter wetting hypothesis and Cassie-Wenzel capillarity-induced wetting transition," *Journal of Colloid and Interface Science*, vol. 311, no. 1, pp. 212–216, 2007.

[4] X. Gao and L. Jiang, "Biophysics: water-repellent legs of water striders," *Nature*, vol. 432, no. 7013, p. 36, 2004.

[5] K. Koch and W. Barthlott, "Superhydrophobic and superhydrophilic plant surfaces: an inspiration for biomimetic materials," *Philosophical Transactions. Series A, Mathematical, Physical, and Engineering Sciences*, vol. 367, no. 1893, pp. 1487–1509, 2009.

[6] C. Neinhuis, "Characterization and distribution of water-repellent, self-cleaning plant surfaces," *Annals of Botany*, vol. 79, no. 6, pp. 667–677, 1997.

[7] T. Wagner, C. Neinhuis, and W. Barthlott, "Wettability and contaminability of insect wings as a function of their surface sculptures," *Acta Zoologica*, vol. 77, no. 3, pp. 213–225, 1996.

[8] B. Bhushan and M. Nosonovsky, "The rose petal effect and the modes of superhydrophobicity," *Philosophical transactions. Series A, Mathematical, Physical, and Engineering Sciences;* vol. 368, no. 1929, pp. 4713–4728, 2010.

[9] B. Bhushan and E. K. Her, "Fabrication of superhydrophobic surfaces with high and low adhesion inspired from rose petal," *Langmuir*, vol. 26, no. 11, pp. 8207–8217, 2010.

[10] R. N. Wenzel, "Resistance of solid surfaces to wetting by water," *Ind. Eng. Chem.*, vol. 28, no. 8, pp. 988–994, 1936.

[11] H. J. Ensikat, P. Ditsche-Kuru, C. Neinhuis et al., "Superhydrophobicity in perfection: the outstanding properties of the lotus leaf," *Beilstein Journal of Nanotechnology*, vol. 2, pp. 152–161, 2011.

[12] C. W. Extrand and S. I. Moon, "Repellency of the lotus leaf: contact angles, drop retention, and sliding angles," *Langmuir*, vol. 30, no. 29, pp. 8791–8797, 2014.

[13] A. B. D. Cassie and S. Baxter, "Wettability of porous surfaces," *Trans. Faraday Soc.*, vol. 40, pp. 546–551, 1944.

[14] L. Gao and T. J. McCarthy, "How Wenzel and Cassie were wrong," *Langmuir*, vol. 23, no. 7, pp. 3762–3765, 2007.

[15] C. W. Extrand and S. I. Moon, "Which controls wetting? Contact line versus interfacial area: simple experiments on capillary rise," *Langmuir*, vol. 28, no. 44, pp. 15629–15633, 2012.

[16] C. W. Extrand, "Remodeling of Super-hydrophobic Surfaces," *Langmuir*, vol. 32, no. 34, pp. 8608–8612, 2016.

[17] H. Y. Erbil, "The debate on the dependence of apparent contact angles on drop contact area or three-phase contact line: A review," *Surface Science Reports*, vol. 69, no. 4, pp. 325–365, 2014.

[18] Y.-T. Cheng, D. E. Rodak, A. Angelopoulos et al., "Microscopic observations of condensation of water on lotus leaves," *Applied Physics Letters*, vol. 87, no. 19, p. 194112, 2005.

[19] C. Dorrer and J. Ruhe, "Condensation and wetting transitions on microstructured ultra-hydrophobic surfaces," *Langmuir : the ACS Journal of Surfaces and Colloids*, vol. 23, no. 7, pp. 3820–3824, 2007.

[20] H. Jo, K. W. Hwang, D. Kim et al., "Loss of superhydrophobicity of hydrophobic micro/nano structures during condensation," *Scientific Reports*, vol. 5, p. 9901, 2015.

[21] R. D. Narhe and D. A. Beysens, "Water condensation on a super-hydrophobic spike surface," *Europhysics Letters (EPL)*, vol. 75, no. 1, pp. 98–104, 2006.

[22] R. Enright, N. Miljkovic, A. Al-Obeidi et al., "Condensation on superhydrophobic surfaces: the role of local energy barriers and structure length scale," *Langmuir*, vol. 28, no. 40, pp. 14424–14432, 2012.

[23] N. Miljkovic, R. Enright, and E. N. Wang, "Modeling and optimization of superhydrophobic condensation," *Journal of Heat Transfer*, vol. 135, no. 11, p. 111004, 2013.

[24] C.-W. Lo, C.-C. Wang, and M.-C. Lu, "Scale effect on dropwise condensation on superhydrophobic surfaces," *ACS Applied Materials & Interfaces*, vol. 6, no. 16, pp. 14353–14359, 2014.

[25] N. Miljkovic, R. Enright, and E. N. Wang, "Effect of droplet morphology on growth dynamics and heat transfer during condensation on superhydrophobic nanostructured surfaces," *ACS Nano*, vol. 6, no. 2, pp. 1776–1785, 2012.